

Understanding Generalization in Adversarial Training via the Bias-Variance Decomposition

Yaodong Yu^{†,*} Zitong Yang^{†,*} Edgar Dobriban[‡] Jacob Steinhardt^{◊,†} Yi Ma[†]

Abstract

Adversarially trained models exhibit a large generalization gap: they can interpolate the training set even for large perturbation radii, but at the cost of large test error on clean samples. To investigate this gap, we decompose the test risk into its bias and variance components. We find that the bias increases monotonically with perturbation size and is the dominant term in the risk. Meanwhile, the variance is unimodal, peaking near the interpolation threshold for the training set. In contrast, we show that popular explanations for the generalization gap instead predict the variance to be monotonic, which leaves an unresolved mystery. We show that the same unimodal variance appears in a simple high-dimensional logistic regression problem, as well as for randomized smoothing. Overall, our results highlight the power of bias-variance decompositions in modern settings—by providing two measurements instead of one, they can rule out some theories and clarify others.

1 Introduction

Adversarial training enhances the robustness of deep neural networks at the cost of decreased accuracy on the clean test samples [Goodfellow et al., 2014, Madry et al., 2017, Sinha et al., 2017]. Though the model can fit the training data perfectly in adversarial training, the generalization error on clean test dataset increases compared with non-adversarially trained models. For example, in the rightmost panel of Figure 1(b), we can see that, even if an adversarially trained model achieves almost zero error on the clean training data (up to a certain level of perturbation ϵ), the error on the clean test data (the blue curve) keeps increasing with ϵ . Hence to improve both robustness and accuracy of (adversarially trained) deep networks, it is crucial to understand the cause for this increased “generalization gap” between errors on the (clean) training dataset and (clean) test dataset.

In this work, to better understand the generalization gap, we turn to a standard tool of statistical learning theory, the bias-variance decomposition [Markov, 1900, Lehmann, 1983, Casella and Berger, 1990, Hastie et al., 2009, Geman et al., 1992]. A large variance corresponds to the instability of the model, whereas a large bias suggests that the model predicts poorly on average. Bias and variance provide more information about the generalization gap than just test error alone: We can better understand whether an explanation works by checking whether it predicts both the bias and variance.

How does adversarial training affect the bias and the variance? A common intuition is that adversarial training (with ℓ_∞ perturbations) intuitively adds small ℓ_∞ boxes around each training sample, making the decision boundary more jagged and complex, and leading to a generalization gap. This intuition is

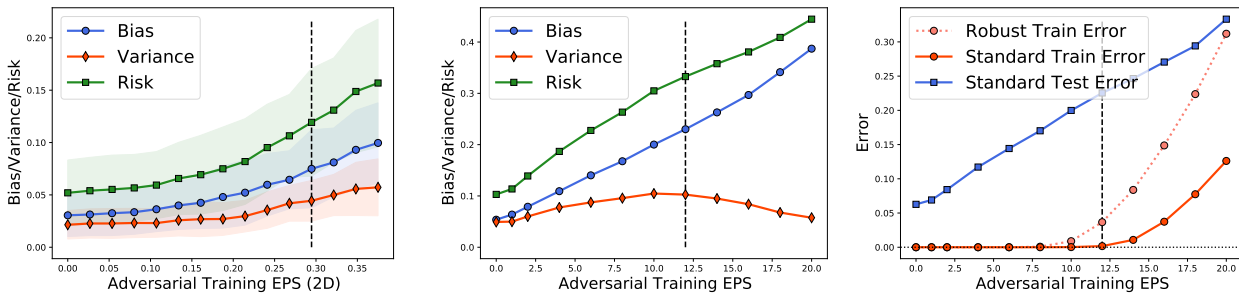
* Yaodong Yu and Zitong Yang contributed equally to this work.

[†] Department of Electrical Engineering and Computer Sciences, University of California, Berkeley.

[◊] Department of Statistics, University of California, Berkeley.

[‡] Department of Statistics, University of Pennsylvania.

Email: yyu@eecs.berkeley.edu, zitong@berkeley.edu, dobriban@wharton.upenn.edu, jsteinhardt@berkeley.edu, yima@eecs.berkeley.edu.



(a) Bias/variance/risk (*2D box example*).

(b) Bias/variance/risk and training/test error (*CIFAR10*).

Figure 1: Measuring performance for ℓ_∞ -adversarial training (with increasing perturbation size) on the *2D box* dataset (1(a)) and *CIFAR10* dataset (1(b)). **Standard error** means the error rate on clean samples, and **robust error** means the error rate on adversarially perturbed samples. The *vertical dashed line* corresponds to the robust training error of the adversarially trained model is larger than 2%. (a) Evaluating the bias, variance, and risk for the ℓ_∞ -adversarially trained model (fully connected network) on the *2D box* dataset. (b) Evaluating bias, variance, risk and robust training error, standard training/test error for the ℓ_∞ -adversarially trained model (WideResNet-28-10) on *CIFAR10* dataset.

commonly presented in the literature, in the form of a simple 2D cartoon that we call the “2D box example” [Madry et al., 2017, Wong and Kolter, 2017, Zhang et al., 2019, Yang et al., 2020b].

In Figure 2, we present two random draws of this 2D box example, which seem to confirm the intuitive explanation. Indeed, although the decision boundaries for different random draws successfully avoid all the boxes, the two boundaries are very different. This suggests that adversarial training increases the variance of the model predictions and thus leads to overfitting. We verify this experimentally in Figure 1(a): variance, as well as bias, monotonically increase with perturbation ε (the box size).

However, we observe a qualitatively different trend on empirical datasets such as CIFAR10. Fig. 1 shows that the variance is instead *unimodal*: it first increases up until the model can no longer robustly interpolate the training set—this location is called the “interpolation threshold”—and then begins to decay. The precise setup of the 2D box example and CIFAR10 experiments will be given in Section 3.1.

This conflict between intuition and practice is reminiscent of the older double-descent mystery [Belkin et al., 2019]. There model variance was intuitively expected to increase, but is instead observed to be unimodal [Yang et al., 2020, Lin and Dobriban, 2020, Adlam and Pennington, 2020, Liu et al., 2020]. The connections are perhaps deeper. Yang et al. [2020] observed that the variance peaks at the interpolation threshold for networks of increasing width. This is analogous to our variance peak, which occurs at the interpolation threshold for increasing ε . As with double descent, the contrast between the simplistic 2D box example and the phenomena on real data suggests that our intuitions and explanations need to be further refined.

To further understand the mechanism behind this bias-variance behavior, we study the synthetic problem of robustly classifying a two-class Gaussian classification model through logistic regression (Section 4). We observe the same increasing bias and unimodal variance shape in this setting. This suggests that the mechanism behind the phenomenon is not tied to deep neural networks. Before the interpolation threshold, the orientation of the separating hyperplane in logistic regression is very sensitive to adversarial perturbations, which leads to increased variance. After the interpolation threshold, a regularization effect (that we elaborate on) kicks in, decreasing the variance.

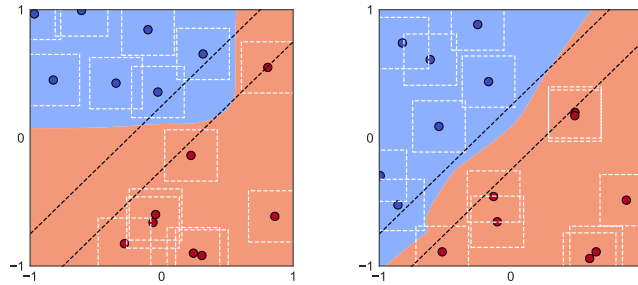


Figure 2: Visualization of decision boundaries of ℓ_∞ adversarially trained models on *2D box example*. The training datasets are randomly sampled from the same data distribution.

Next, we study if the observed shape of increasing bias and unimodal variance in adversarial training holds for other robust training procedures. We consider randomized smoothing training [Lecuyer et al., 2019, Cohen et al., 2019] which effectively adds Gaussian noise to each mini-batch in the SGD iterations. We observe similar shapes of bias and variance as in adversarial training (Section 3). Intriguingly, if we instead freeze the Gaussian noise for each training sample, i.e., we perturb each sample only once in the beginning, the variance instead increases monotonically, as in the 2D example. This again demonstrates the power of having two measurements: If we only look at the test error, randomized smoothing and training on Gaussian-perturbed data appear to be the same, but more measurements allow us to distinguish them.

In addition to our main findings above, we propose a generalized form of *adversarial bias-variance decomposition* under adversarial perturbation at test time (Section 2). We find that the *adversarial bias* is usually much larger than the *adversarial variance*. This suggests that the adversarial attack produces the same, incorrect label for different models, which could help understand and explain the transferability of adversarial attacks [Liu et al., 2016, Tramèr et al., 2017].

1.1 Related work

Robustness-accuracy tradeoff. There is a large literature on understanding the trade-off between adversarial robustness and standard accuracy for adversarially robust classification problems. Classical works [Xu et al., 2009b,a] study robustness of linear models, showing equivalences between adversarially robust regression and lasso. Fawzi et al. [2018], Zhang et al. [2019], Dobriban et al. [2020] identified the fundamental robustness-accuracy trade-off in simplified theoretical models, where samples from different classes are close and there does not exist a robust and accurate classifier. Nakkiran [2019] argue theoretically that the tradeoff is due to the simplicity of the classifiers, which suggested that more complex classifiers are required for adversarial robustness. Tsipras et al. [2018] and Ilyas et al. [2019] approach this trade-off from a different angle. They demonstrate that adversarially robust models are less accurate because robust models cannot rely on predictive, yet non-robust features of the data. Dan et al. [2020], Javanmard et al. [2020], Javanmard and Soltanolkotabi [2020], Dobriban et al. [2020], Megyeri et al. [2019] study the trade-off for linear models and provide a precise characterization of the robust error. Raghunathan et al. [2020] argue that unlabeled data can be used to mitigate the trade-off and improve model robustness. Yang et al. [2020b] empirically study the trade-off via local Lipschitzness. Other works study robustness for non-parametric methods [Wang et al., 2018, Bhattacharjee and Chaudhuri, 2020, Yang et al., 2020a].

Adversarially robust generalization. Schmidt et al. [2018] consider a Gaussian classification model and demonstrate that adversarial training requires more data for generalization. Cullina et al. [2018], Attias et al. [2019], Yin et al. [2019], Khim and Loh [2018], Montasser et al. [2019] study the generalization and sample complexity via Rademacher complexity and VC dimension. Bubeck et al. [2018, 2019] argue that learning robust classifiers may be computationally hard. Another line of work [Javanmard and Soltanolkotabi, 2020, Dan et al., 2020, Dobriban et al., 2020, Taheri et al., 2020] studies statistical properties of adversarial logistic regression. Several works use the concentration of measure to study the existence of adversarial examples in high dimensions [Gilmer et al., 2018, Shafahi et al., 2019, Mahloujifar et al., 2019]. Similarly, some works develop connections to optimal transport [Dohmatob, 2019, Bhagoji et al., 2019, Pydi and Jog, 2020].

Adversarial defenses and attacks. A large body of literature is devoted to improving adversarial robustness [Goodfellow et al., 2014, Kurakin et al., 2016, Madry et al., 2017, Hein and Andriushchenko, 2017, Wong and Kolter, 2017, Sinha et al., 2017, Cohen et al., 2019, Raghunathan et al., 2018] and developing adversarial attacks [Carlini and Wagner, 2017, Papernot et al., 2017, Athalye et al., 2018, Kang et al., 2019, Aboutaleb et al., 2020, Croce and Hein, 2020]. Carmon et al. [2019], Uesato et al. [2019], Najafi et al. [2019], Zhai et al. [2019] argue that using unlabeled data can improve model adversarial robustness. Shah et al. [2020] show that the ‘‘Simplicity Bias’’ in deep neural networks could be one possible explanation of the existence of universal adversarial examples. Gowal et al. [2020] show that by exploring the model size, activation function, and model weight averaging, adversarial training can achieve state-of-the-art ℓ_∞/ℓ_2 adversarial robustness on the CIFAR10 dataset. Croce et al. [2020] recently benchmark adversarial ℓ_2/ℓ_∞ robustness based on AutoAttack [Croce and Hein, 2020].

2 Preliminary

We review the standard bias-variance decomposition and also propose an *adversarial* bias-variance decomposition that will be used in later sections. We mainly consider the bias-variance decomposition of the squared ℓ_2 loss; extensions to the cross-entropy loss can be found in Appendices A and C.

Standard training and adversarial training. For standard supervised learning tasks, given n i.i.d. training samples $\mathcal{T} = \{(\mathbf{x}_i, \mathbf{y}_i)\}_{i=1}^n$, one-hot encoding vector \mathbf{y}_i , a parameterized class of prediction functions $f_\theta(\cdot)$, and a loss function $\ell(\cdot, \cdot)$, the goal of *standard training* is finding $\hat{\theta}(\mathcal{T})$ that approximately solves the following problem:

$$\min_{\theta} \frac{1}{n} \sum_{i=1}^n \ell(f_\theta(\mathbf{x}_i), \mathbf{y}_i). \quad (1)$$

Deep models learned through Eq. (1) are vulnerable to adversarial perturbations [Szegedy et al., 2013, Biggio et al., 2013]. *Adversarial training* (AT) enhances the robustness of the model by solving the following robust optimization problem:

$$\min_{\theta} \frac{1}{n} \sum_{i=1}^n \max_{\delta_i \in \Delta} \ell(f_\theta(\mathbf{x}_i + \delta_i), \mathbf{y}_i). \quad (2)$$

In practice, the inner maximization problem is approximately solved by projected gradient descent (PGD), and the outer minimization problem is approximately solved by stochastic gradient descent (SGD) [Madry et al., 2017]. We follow this adversarial training procedure in this paper. A typical choice

for the perturbation set is the ℓ_p norm ball $\Delta = \{\boldsymbol{\delta} : \|\boldsymbol{\delta}\|_p \leq \varepsilon\}$. More precisely, to find the adversarial perturbation $\boldsymbol{\delta}$ for data point (\mathbf{x}, \mathbf{y}) on the model $f_{\hat{\boldsymbol{\theta}}(\mathcal{T})}$, we approximately solve the optimization:

$$\boldsymbol{\delta}(\mathbf{x}, \mathbf{y}, \mathcal{T}) \in \arg \max_{\boldsymbol{\delta} \in \Delta} \ell \left(f_{\hat{\boldsymbol{\theta}}(\mathcal{T})}(\mathbf{x} + \boldsymbol{\delta}), \mathbf{y} \right). \quad (3)$$

Bias-variance decomposition. Given a generic test point (\mathbf{x}, \mathbf{y}) , an accurately trained model satisfies $\mathbf{y} \approx f_{\hat{\boldsymbol{\theta}}}(\mathbf{x})$. Therefore, for a good model, the prediction $f_{\hat{\boldsymbol{\theta}}}(\mathbf{x})$ does not depend too much on the training set \mathcal{T} . This is can be quantified by the variance:

$$\text{Var} = \mathbb{E}_{\mathbf{x}} \text{Var}_{\mathcal{T}} \left[f_{\hat{\boldsymbol{\theta}}(\mathcal{T})}(\mathbf{x}) \right].$$

Here we consider the random design variance. A large variance implies that the trained model $f_{\hat{\boldsymbol{\theta}}}$ is sensitive to a particular realization of the training dataset \mathcal{T} , which is unfavorable. The bias term is

$$\text{Bias} = \mathbb{E}_{\mathcal{T}, \mathbf{x}, \mathbf{y}} \left\| \mathbf{y} - f_{\hat{\boldsymbol{\theta}}(\mathcal{T})}(\mathbf{x}) \right\|_2^2 - \text{Var}.$$

Adversarial bias-variance. Throughout this paper, we mainly study the standard bias-variance decomposition for neural networks, but we also propose a generalized bias-variance decomposition, the *adversarial bias-variance decomposition*, to help us investigate the behavior of adversarial attacks. A challenge is that in the adversarial setting, we not only need to take into account the prediction at a particular test point \mathbf{x} , but also at a point $\mathbf{x}' = \mathbf{x} + \boldsymbol{\delta}$, where $\boldsymbol{\delta} \in \Delta$ is the attack from Eq. (3).

For a robust model, $f_{\hat{\boldsymbol{\theta}}(\mathcal{T})}(\mathbf{x} + \boldsymbol{\delta}(\mathbf{x}, \mathbf{y}, \mathcal{T}))$ should still be a good predictor of the label \mathbf{y} . Therefore, as in the standard training setting, the prediction $f_{\hat{\boldsymbol{\theta}}}(\mathbf{x} + \boldsymbol{\delta}(\mathbf{x}, \mathbf{y}, \mathcal{T}))$ should not depend too much on \mathcal{T} . We can measure how much the prediction depends on \mathcal{T} by computing the adversarial variance

$$\text{AVar} = \mathbb{E}_{\mathbf{x}, \mathbf{y}} \text{Var}_{\mathcal{T}} \left[f_{\hat{\boldsymbol{\theta}}(\mathcal{T})}(\mathbf{x} + \boldsymbol{\delta}(\mathbf{x}, \mathbf{y}, \mathcal{T})) \right].$$

The adversarial bias can be analogously defined as

$$\text{ABias} = \mathbb{E}_{\mathbf{x}, \mathbf{y}} \left[\left\| \mathbf{y} - \mathbb{E}_{\mathcal{T}} f_{\hat{\boldsymbol{\theta}}(\mathcal{T})}(\mathbf{x} + \boldsymbol{\delta}(\mathbf{x}, \mathbf{y}, \mathcal{T})) \right\|^2 \right].$$

One can check that the sum of bias and variance gives the expected risk:

$$\text{AR} = \mathbb{E}_{\mathcal{T}} \mathbb{E}_{\mathbf{x}, \mathbf{y}} \left[\max_{\boldsymbol{\delta} \in \Delta} \left\| f_{\hat{\boldsymbol{\theta}}}(\mathbf{x} + \boldsymbol{\delta}) - \mathbf{y} \right\|^2 \right],$$

which can be decomposed as

$$\underbrace{\mathbb{E}_{\mathbf{x}, \mathbf{y}} \text{Var}_{\mathcal{T}} \left[f_{\hat{\boldsymbol{\theta}}}(\mathbf{x} + \boldsymbol{\delta}_{\mathcal{T}}) \right]}_{\text{Adversarial Variance}} + \underbrace{\mathbb{E}_{\mathbf{x}, \mathbf{y}} \left[\left\| \mathbf{y} - \mathbb{E}_{\mathcal{T}} f_{\hat{\boldsymbol{\theta}}}(\mathbf{x} + \boldsymbol{\delta}_{\mathcal{T}}) \right\|^2 \right]}_{\text{Adversarial Bias}}, \quad (4)$$

where $\boldsymbol{\delta}_{\mathcal{T}}$ is short for $\boldsymbol{\delta}(\mathbf{x}, \mathbf{y}, \mathcal{T})$. The advantage of our definition of variance is that it directly measures the variation of the model's prediction at test sample \mathbf{x} in presence of adversarial perturbation. An algorithm for estimating the variance given a single training dataset \mathcal{T} at a particular test point (\mathbf{x}, \mathbf{y}) is given in Algorithm 1 in Appendix A.

3 Measuring Bias and Variance for Deep Neural Networks

In this section, we study the bias-variance behavior of deep neural networks trained by various methods. For adversarial training on the CIFAR10 dataset, we find that *the variance is unimodal and the bias is monotonically increasing* (Figure 1(b)) as a function of the increasing perturbation size. This is different from the 2D box example (Figure 1(a)). We then study the connection between adversarial training and other training approaches such as randomized smoothing. Our code is available at <https://github.com/yaodongyu/BiasVariance-AdversarialTraining>.

Bias-variance evaluation setup. To evaluate the bias and variance, we partition the training dataset \mathcal{T} into two disjoint parts $\mathcal{T} = \mathcal{T}_1 \cup \mathcal{T}_2$. We evaluate the bias-variance decomposition for the mean squared error $\|\mathbf{y} - f_{\hat{\theta}}(\mathbf{x})\|^2$ (Section 2), where \mathbf{y} is the one-hot encoding label vector and $f_{\hat{\theta}}(\mathbf{x})$ is the output of the softmax layer. More details for estimating the bias and the variance can be found in Appendix A.

3.1 Adversarially Trained Models

We first study the bias-variance decomposition for ℓ_{∞} adversarially trained models with increasing perturbation size ε on the synthetic 2D box dataset (in Figure 1(a)) and CIFAR10 dataset (Figure 1(b)).

2D box example experimental setup. We uniformly sample the input \mathbf{x} is from

$$\left\{ \mathbf{x} : -1 \leq x_1, x_2 \leq 1, |x_1 - x_2| \geq \gamma/\sqrt{2} \right\},$$

and the label for \mathbf{x} is $y = \text{sign}(x_2 - x_1)$, where $\gamma \in (0, 1)$ is the margin parameter. Figure 1 includes two random training datasets for this 2D box example. We set the margin $\gamma = 1/(4\sqrt{2})$, the number of training sample $n = 40$, and the number of test samples as 10,000. We perform ℓ_{∞} adversarial training using a fully connected network (3 hidden layers with 100 nodes for each hidden layer). We vary the adversarial perturbation ε from 0.0 to $\gamma \cdot 2\sqrt{2}$, and the perturbation step size for 10-step-PGD is set to be $\eta = \varepsilon \cdot 0.4$. We use the Adam [Kingma and Ba, 2014] optimizer for 2,000 epochs with a learning rate of 0.001.

CIFAR10 experimental setup. We use the Wide-ResNet architecture (WRN-28-10) [Zagoruyko and Komodakis, 2016] for the CIFAR10 dataset [Krizhevsky and Hinton, 2009]. We train our models using stochastic gradient descent (SGD) with momentum 0.9, where the learning rate is 0.1, mini-batch size is 128, and the weight decay parameter is 0.0005. We train the models for 200 epochs and apply stage-wise learning rate decay during training, where we decay the learning rate by a factor of 0.1 at epochs 100 and 150. These architecture and training parameters are commonly used in ℓ_{∞} PGD adversarial training on CIFAR10 [Madry et al., 2017, Rice et al., 2020]. We consider the perturbation size $\varepsilon/255$ and vary ε from 0 to 20. For the inner maximization in adversarial training, we apply a 10-step PGD attack with perturbation step size $\eta = 0.25 \cdot (\varepsilon/255)$.

In addition to the model trained to converge approximately, we study the bias-variance decomposition of early stopping models. Early stopping is a widely used technique in adversarial training for improving model robustness to adversarial perturbations [Zhang et al., 2019, Rice et al., 2020, Goyal et al., 2020]. We denote the training stopped at the 100-th epoch as the “*early stopping*” model.

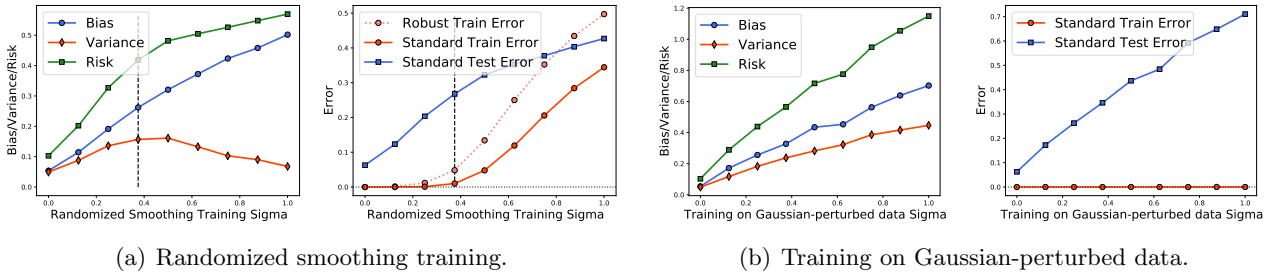


Figure 3: Measure bias/variance/risk and train/test error for *randomized smoothing training* and *training on Gaussian-perturbed data* on the CIFAR10 dataset using WRN-28-10 with different σ^2 . (a) Results for randomized smoothing training. (b) Results for training on Gaussian-perturbed data.

Bias-variance behavior on CIFAR10. From Figure 1(b), we find that the bias increases monotonically when we increase the perturbation size ε . Compared with the variance, the bias is the dominant term in the risk. We also observe that the variance first increases to a peak and then decreases with the perturbation size, and the location of the peak is close to the robust interpolation threshold (i.e., robust training error is nearly zero) for the training set. The decreased variance phenomenon aligns well with the non-robust features perspective studied in Tsipras et al. [2018], Ilyas et al. [2019]. From the non-robust feature perspective, training with larger epsilon values would bias the model towards simpler features that are easier to learn, hence decreasing variance. We further study the behavior of bias and variance in a simple linear model in Section 4.

Adversarial training on CIFAR10 v.s. 2D box example. As shown in Figure 1(a) (2D box example) and Figure 1(b) (CIFAR10), we observe that on the CIFAR10 dataset, the risk and bias are monotonically increasing and the variance is unimodal when increasing the adversarial perturbation ε . The behavior of the bias and the risk of the 2D box example in Figure 1(a) is similar to the CIFAR10 setting. However, *the variance of the 2D box example is different from the CIFAR10 result*: the variance of the 2D box example is monotonically increasing w.r.t. the perturbation ε .

Early stopping. As shown in Figure 4, the peak of the variance curve of early stopped models is smaller than the variance peak without early stopping. For early stopped models, we find that the bias dominates the risk, and the variance is relatively smaller. If we consider the same adversarial perturbation ε with and without early stopping, the variance of the non-early-stopped models is larger than the early stopped models, whereas the bias and the risk decrease when trained with more epochs.

In summary, by measuring the bias-variance decomposition on the synthetic and real datasets, we find that the behavior of variance on the real dataset is different from the 2D box example. Meanwhile, we observe the characteristic shape of the bias and variance for adversarial training: the variance is unimodal and the bias is monotonically increasing with perturbation size. The unimodal variance phenomenon is also observed in ℓ_∞ and ℓ_2 adversarial training on the CIFAR10 and CIFAR100 datasets, and the results can be found in Appendix C.

3.2 Training with Gaussian Noise

In this subsection, we study the bias-variance decomposition for other training approaches on the CIFAR10 dataset: randomized smoothing training and training on Gaussian-perturbed data. Randomized smoothing training [Lecuyer et al., 2019, Cohen et al., 2019] is another form of robust training procedure,

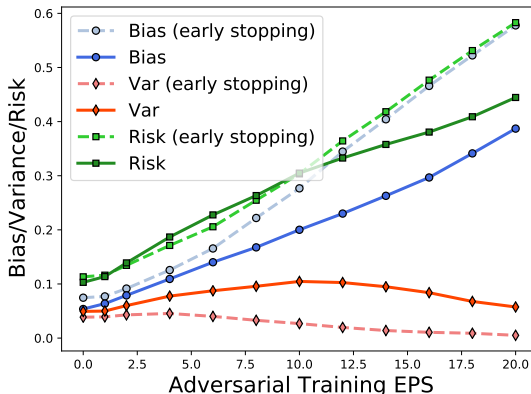


Figure 4: For ℓ_∞ adversarial training on the CIFAR10 dataset, comparing the bias, variance, and risk for early stopped models and non-early-stopped models.

which adds random Gaussian noise to each mini-batch used for the SGD updates. In contrast, the training on Gaussian-perturbed data adds Gaussian noise to training images before training and fix the noise for every training image during training, which can be viewed as a distributional shift of the training dataset. We evaluate the bias and variance for these two training methods and compare their behavior with ℓ_∞ adversarial training. We perturb the training images with random Gaussian noise with variance $\sigma^2 \in [0.0, 1.0]$ and clip pixels to $[0.0, 1.0]$. We discuss the detail of the experiment setup in Appendix C.1.

Comparing randomized smoothing training to AT. As shown in Figure 3(a) and Figure 6, we find that *models trained with randomized smoothing behave similarly to adversarially trained models* in terms of the shape of the bias and variance with increasing perturbation size. More specifically, in Figure 3(a), when increasing the training noise variance σ^2 for randomized smoothing, the standard bias is monotonically increasing and the standard variance is unimodal. Similar to adversarial training, the peak of the variance for randomized smoothing training is close to the interpolation threshold.

Comparing training on Gaussian-perturbed data to AT. For the results of training on Gaussian-perturbed data in Figure 3(b), *both the bias and variance are monotonically increasing* when we increase the perturbation noise variance σ^2 to the training inputs. The training on Gaussian-perturbed data is different from adversarial training with respect to the shape of the variance. This suggests that, in comparison with randomized smoothing, *training on Gaussian-perturbed data may not be a good proxy for understanding adversarial training*.

In comparison to the bias-variance shape of adversarial training, we find that randomized smoothing training is similar to adversarial training, whereas the training on Gaussian-perturbed data behaves differently from the above two training methods. Although the risk curve of both randomized smoothing training and training on Gaussian-perturbed data is monotonically increasing, the bias-variance decomposition enables us to distinguish these two training methods. Moreover, we also observe the “peak near interpolation threshold” for randomized smoothing training.

3.3 Adversarial Bias-variance Decomposition

In addition to standard bias-variance decomposition, we also study the adversarial bias-variance decomposition (defined in Eq. (4)) for adversarial training and randomized smoothing training on the CIFAR10

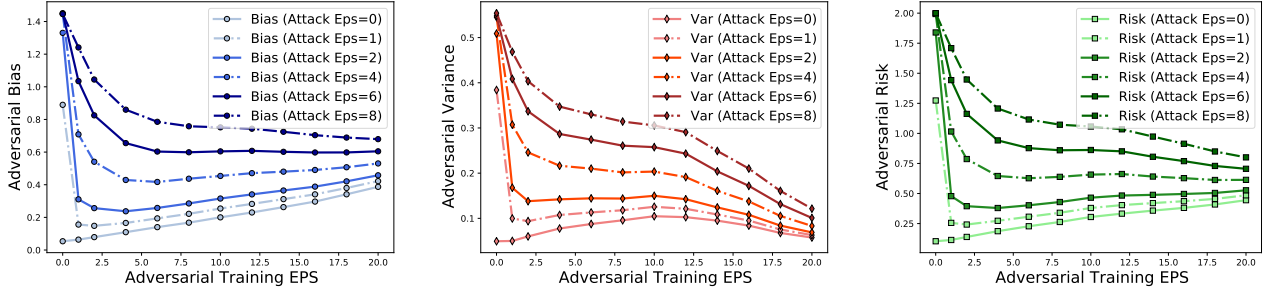


Figure 5: Adversarial bias, variance, and risk for ℓ_∞ adversarially trained models on the CIFAR10 dataset using WRN-28-10. Each curve corresponds to the ε -adversarial bias-variance decomposition, and the EPS represents the $\ell_\infty = \text{EPS}/255.0$ PGD attack. **(Left)** Adversarial bias. **(Middle)** Adversarial variance. **(Right)** Adversarial risk.

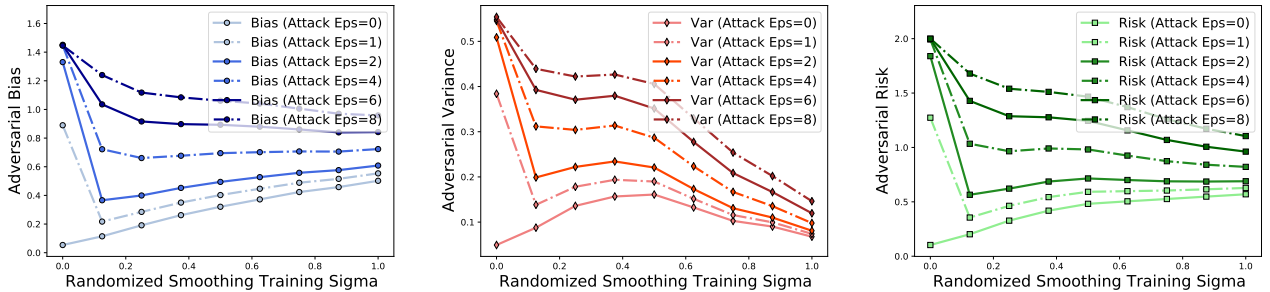


Figure 6: Adversarial bias, variance, and risk for *randomized smoothing training* models on the CIFAR10 dataset using WRN-28-10. Each curve corresponds to the ε -adversarial bias-variance decomposition, and the EPS represents the $\ell_\infty = \text{EPS}/255.0$ PGD attack. **(Left)** Adversarial bias. **(Middle)** Adversarial variance. **(Right)** Adversarial risk.

dataset. We apply the same training dataset partition procedure as bias-variance decomposition. To approximately find $\delta\tau$ defined in Eq. (4), we use the ℓ_∞ -PGD adversarial attack for generating the adversarial perturbations, where the number of perturb step is 20 and the step size is $\eta = 0.15 \cdot (\varepsilon/255)$.

The results for the ℓ_∞ adversarially trained models are summarized in Figure 5. With increasing perturbation size for evaluating the adversarial bias and variance, the adversarial bias curve is changed from monotone increasing to monotone decreasing, and the variance curve is changed from unimodal to monotone decreasing. The adversarial variance is relatively small compared with the adversarial bias under various attack radii; similar to the standard bias-variance results in Figure 1(b). Furthermore, from Figure 6, we observe that models trained with randomized smoothing have similar characteristic adversarial bias-variance curve shapes as adversarially trained models (in Figure 5): the adversarial variance under all adversarial perturbations becomes smaller when increasing the training variance σ^2 , and the bias shape is changed from monotone increasing to monotone decreasing with increased adversarial perturbation ε .

More experimental results. We also study ℓ_∞ and ℓ_2 adversarial training on the CIFAR10 and CIFAR100 datasets, where we observe similar phenomena of unimodal variance and monotonically increasing bias. Moreover, we investigate the bias-variance decomposition on out-of-distribution datasets. See Appendix C for more experimental results.

4 Linear Models

In this section, we consider two linear models that serve different purposes for the paper. First, we study adversarial training in the setting of logistic regression. We demonstrate that in this simplified setting, we can already observe the characteristic shape of bias and variance. In the second part, we study linear regression with adversarial training and randomized smoothing training. We argue that both training schemes amount to adding a shrinkage factor to the ground truth linear parameters. This gives an intuitive explanation of why the variance has similar behavior in those two settings, as discussed in Section 3.

4.1 Logistic Regression

To further understand the unimodal variance and increasing bias proposed in Section 3.1. We consider a standard setup for logistic regression where we can solve the minimax optimization problem exactly. We can still observe the characteristic shape of bias and variance in this simple setting. This implies that the proposed shape is not tied to deep learning.

Data Generative Model. We assume that the data is generated according to a mixture of Gaussian distributions. For $i = 1, \dots, n$, each pair of training samples $\mathbf{x}_i \in \mathbb{R}^d$ and $y_i \in \{-1, 1\}$ has distribution

$$y_i \sim \text{Bernoulli}(0.5), \quad \mathbf{x}_i | y_i \sim \mathcal{N}(y_i \mathbf{v}, \sigma^2 \mathbf{I}_d), \quad (5)$$

where $\mathbf{v} = [1, 1, \dots, 1] / \sqrt{d} \in \mathbb{R}^d$ specifies the center of the cluster.

Loss Function. We use the standard cross-entropy loss

$$R^{(n)}(\boldsymbol{\theta}) = \frac{1}{n} \sum_{i=1}^n \ell(y_i \langle \mathbf{x}_i, \boldsymbol{\theta} \rangle),$$

where $\ell(z) = \log(1 + e^{-z})$. The inner maximization problem (using ℓ_2 perturbation) in the adversarial loss can be solved exactly:

$$\text{AR}^{(n)}(\boldsymbol{\theta}) = \frac{1}{n} \sum_{i=1}^n \log \left(1 + e^{-y_i \langle \mathbf{x}_i, \boldsymbol{\theta} \rangle + \varepsilon \|\boldsymbol{\theta}\|_2} \right). \quad (6)$$

Adversarial training amounts to solve the convex program

$$\hat{\boldsymbol{\theta}}_n = \arg \min_{\boldsymbol{\theta}} \text{AR}^{(n)}(\boldsymbol{\theta}).$$

Given a test data-point (\mathbf{x}, y) , the risk is

$$R(\hat{\boldsymbol{\theta}}_n) = \mathbb{E}_{\mathbf{x}, y} \ell(y \langle \hat{\boldsymbol{\theta}}_n, \mathbf{x} \rangle).$$

We consider a definition of bias and variance specifically designed for logistic loss:

$$\text{Bias} = \mathbb{E}_{\mathbf{x}, y} \log Z_{\mathbf{x}} + \mathbb{E}_{\hat{\boldsymbol{\theta}}_n} R(\hat{\boldsymbol{\theta}}_n), \quad \text{Var} = -\mathbb{E}_{\mathbf{x}} \log Z_{\mathbf{x}},$$

where

$$Z_{\mathbf{x}} = \exp \left[-\mathbb{E}_{\hat{\boldsymbol{\theta}}_n} \ell(\langle \hat{\boldsymbol{\theta}}_n, \mathbf{x} \rangle) \right] + \exp \left[-\mathbb{E}_{\hat{\boldsymbol{\theta}}_n} \ell(-\langle \hat{\boldsymbol{\theta}}_n, \mathbf{x} \rangle) \right].$$

The derivation of the formulas above is deferred to Appendix D.1, where we also prove in Proposition 3 that the proposed notion of variance has the usual property of being non-negative, and equal to 0 only when $\hat{\boldsymbol{\theta}}_n$ is non-random.

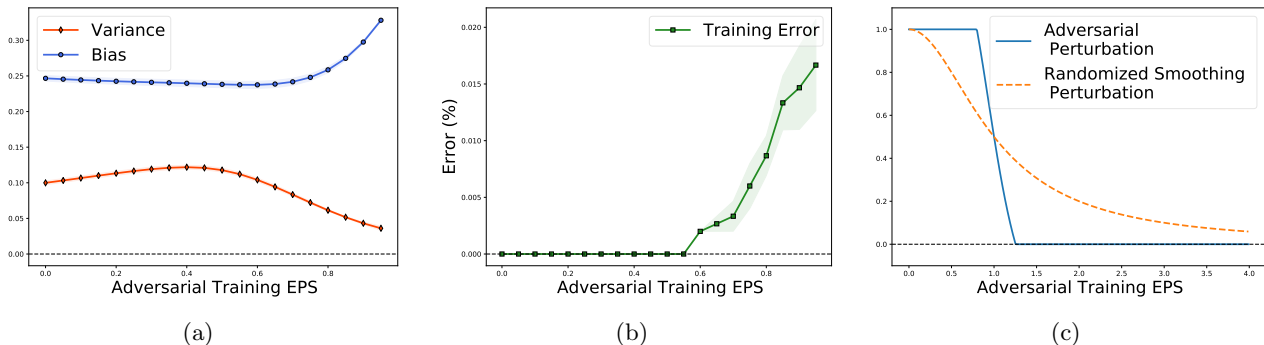


Figure 7: **Left:** Bias and variance for adversarially trained logistic regression with mixture of Gaussian data. **Middle:** The corresponding test error for the logistic regression. **Right:** Comparison of the shrinkage factor for linear regression with adversarial and random perturbation.

Behavior of Bias and Variance. Given the above setup, we see in Figure 7(a) that, as a function of ε , the variance is indeed unimodal and the bias is increasing. We set the number of training samples $n = 100$, the data dimension $d = 100$, the cluster radius (variance of the Gaussian mixture) $\sigma = 0.7$. When ε is relatively small, we are able to perfectly separate the two classes. As ε increases, we eventually encounter a threshold where we can not interpolate the training data. In Figure 7(a), we see that the interpolation threshold is around $\varepsilon = 0.4$, which corresponds to the variance peak in Figure 7(a).

Before the interpolation threshold, the classifier separates the data even with adversarial perturbations. This leads to high variation in the orientation of the separating hyperplane. In the adversarial logistic loss in equation (6), the loss function penalizes a large norm of θ . After the threshold, this regularization effect kicks in and effectively reduces the variance. The connection between adversarial training and norm-based regularization has been discussed in Li et al. [2019], but this perspective alone does not clarify the initial increase in the variance.

4.2 Linear Regression

In Section 3, we find that randomized smoothing training and adversarial training have similar bias-variance shapes. To understand the similarities and differences between these two training strategies more carefully, we study linear regression with randomized smoothing and adversarial training.

Since the goal is to understand the effect of increasing ε , we consider a simplified setting where the number of samples $n \rightarrow \infty$. In other words, we study the parameter θ that could minimize the test time loss of adversarial and randomized smoothing loss functions. Existing results show that both training schemes can be interpreted as a multiplicative shrinkage factor to the ground truth parameters. This also gives an intuitive explanation of why these two training methods eventually decrease the variance and increase the bias: As ε gets larger, the training scheme tends to be biased toward the null estimator.

Data Generative Model. We assume the data has distribution $\mathbf{x} \sim \mathcal{N}(0, I_d)$, $y|\mathbf{x} = \langle \mathbf{x}, \theta_0 \rangle$ for some underlying true parameter $\theta_0 \in \mathbb{R}^d$.

Adversarial Linear Regression. Given θ , the adversarial risk (AR) is

$$\text{AR}(\theta) = \mathbb{E}_{\mathbf{x}} \max_{\|\delta\| \leq \varepsilon} (\langle \mathbf{x}_i + \delta, \theta \rangle - y_i)^2. \quad (7)$$

The next proposition states the θ that minimizes the adversarial risk.

Proposition 1 (Proposition 1, Xing et al. [2020]). *The optimal shrinkage for adversarial linear regression with ℓ_2 perturbation is $c(\varepsilon)$, where*

$$c(\varepsilon) = \begin{cases} 1 & \varepsilon \leq \sqrt{\frac{2}{\pi}}, \\ \frac{1-\varepsilon\sqrt{2/\pi}}{1-2\varepsilon\sqrt{2/\pi}+\varepsilon^2} & \sqrt{\frac{2}{\pi}} \leq \varepsilon \leq \sqrt{\frac{\pi}{2}}, \\ 0 & \sqrt{\frac{\pi}{2}} \leq \varepsilon. \end{cases}$$

Mathematically, $c(\varepsilon)\boldsymbol{\theta}_0 = \arg \min_{\boldsymbol{\theta}} AR(\boldsymbol{\theta})$.

A plot of the curve $c(\varepsilon)$ above can be found in 7(c) where we see that it shrinks $\boldsymbol{\theta}$ toward $\mathbf{0}$.

Randomized Smoothing Linear Regression. We consider the same setup except that the perturbation $\boldsymbol{\delta} \stackrel{\text{i.i.d.}}{\sim} \mathcal{N}(0, \varepsilon^2 \mathbf{I}_d)$ is sampled from an isotropic Gaussian distribution [Lecuyer et al., 2019, Cohen et al., 2019]. In this case, the randomized smoothing risk (RSR) is

$$\text{RSR}(\boldsymbol{\theta}) = \mathbb{E}_{\mathbf{x}, \boldsymbol{\delta}} (\langle \boldsymbol{\theta}, \mathbf{x} + \boldsymbol{\delta} \rangle - y)^2 = \mathbb{E}_{\mathbf{x}} (\langle \boldsymbol{\theta}, \mathbf{x} \rangle - y)^2 + \varepsilon^2 \|\boldsymbol{\theta}\|_2^2.$$

The fact that training with random noise is equivalent to ridge regression dates back to Bishop [1995], Chapelle et al. [2001]. The next proposition then follows from well-known results on the shrinkage factor of ridge regression e.g. Section 3.4 in Hastie et al. [2015].

Proposition 2 (Optimal Shrinkage for Randomized Smoothing). *The optimal shrinkage factor for linear regression with randomized smoothing is $\frac{1}{1+\varepsilon^2}$. Mathematically,*

$$\frac{1}{1+\varepsilon^2}\boldsymbol{\theta}_0 = \arg \min_{\boldsymbol{\theta}} \text{RSR}(\boldsymbol{\theta}).$$

This shows that randomized smoothing also adds a shrinkage factor to the ground truth parameter $\boldsymbol{\theta}_0$. A comparison between the shrinkage factors for randomized smoothing and adversarial perturbation can be seen in Figure 7(c). We see a quantitative difference between the two methods: The randomized smoothing shrinkage is more smooth and slowly decaying than adversarial shrinkage, which in contrast displays some “hard thresholding” behavior.

5 Discussion and Future Works

In this paper, we showed that popular intuition around adversarial training needs to be modified—while the 2D box picture provides an appealing explanation for the generalization gap, it does not fully account for behavior in high dimensions. To discover this, we needed to look at the bias and variance, as opposed to only the test error. This highlights the power of multiple measurements, as they provide a tighter sieve through which explanations must pass.

Implications for adversarial training. Our results also provide a jumping-off point for reducing the adversarial generalization gap. They show that the gap is mainly due to bias, thus pinpointing the locus for improvement. The large bias is counterintuitive, as it occurs even when the training error is zero, which usually instead corresponds to low bias and high variance. This suggests that adversarial training imposes a strong form of *implicit regularization* [Neyshabur et al., 2014] that causes the bias. A better understanding of this regularization could perhaps help us design better architectures to accommodate adversarial training.

A conjecture. In addition, our results lend further support to the theory that the *variance peak* and the *interpolation threshold* are closely connected. Recall that our variance curves consistently reach their maximum near the point where the robust training error becomes non-zero. This echoes results in Yang et al. [2020], who found the same phenomenon for regular training with models of increasing width. This leads us to the following conjecture:

Conjecture 1. *If we perturb our model (e.g. increase regularization) in a way that results in an interpolation threshold, the variance will change monotonicity at the interpolation threshold.*

We expect the conjecture to hold when we vary other parameters, e.g. number of samples, level of regularization such as early stopping. Our conjecture contrasts with the “generalized double descent” in Nakkiran et al. [2020], which instead predicts that the test error peaks at the interpolation threshold. While the test error and variance peaks are often nearby for models exhibiting double descent, our experience is that the variance peak more closely and consistently coincides with the interpolation threshold. Moreover, only some models exhibit double descent, while almost all high-dimensional models have a variance peak [Yang et al., 2020]. If this conjecture is true, it merits further explanation. Why are the peak and interpolation threshold so closely tied?

Acknowledgements

We would like to thank Preetum Nakkiran, Aditi Raghunathan, and Dimitris Tsipras for their valuable feedback and comments.

References

- Hossein Aboutaleb, Mohammad Javad Shafiee, Michelle Karg, Christian Scharfenberger, and Alexander Wong. Vulnerability under adversarial machine learning: Bias or variance?, 2020.
- Ben Adlam and Jeffrey Pennington. Understanding double descent requires a fine-grained bias-variance decomposition. *arXiv preprint arXiv:2011.03321*, 2020.
- Anish Athalye, Nicholas Carlini, and David Wagner. Obfuscated gradients give a false sense of security: Circumventing defenses to adversarial examples. In *International Conference on Machine Learning*, pages 274–283. PMLR, 2018.
- Idan Attias, Aryeh Kontorovich, and Yishay Mansour. Improved generalization bounds for robust learning. In *Algorithmic Learning Theory*, pages 162–183. PMLR, 2019.
- Mikhail Belkin, Daniel Hsu, Siyuan Ma, and Soumik Mandal. Reconciling modern machine-learning practice and the classical bias–variance trade-off. *Proceedings of the National Academy of Sciences*, 116(32):15849–15854, 2019. ISSN 0027-8424. doi: 10.1073/pnas.1903070116. URL <https://www.pnas.org/content/116/32/15849>.
- Arjun Nitin Bhagoji, Daniel Cullina, and Prateek Mittal. Lower bounds on adversarial robustness from optimal transport. In *Advances in Neural Information Processing Systems*, pages 7496–7508, 2019.
- Robi Bhattacharjee and Kamalika Chaudhuri. When are non-parametric methods robust? In *International Conference on Machine Learning*, 2020.

- Battista Biggio, Iginio Corona, Davide Maiorca, Blaine Nelson, Nedim Šrndić, Pavel Laskov, Giorgio Giacinto, and Fabio Roli. Evasion attacks against machine learning at test time. In *Joint European conference on machine learning and knowledge discovery in databases*, pages 387–402. Springer, 2013.
- Chris M Bishop. Training with noise is equivalent to tikhonov regularization. *Neural computation*, 7(1): 108–116, 1995.
- Sébastien Bubeck, Yin Tat Lee, Eric Price, and Ilya Razenshteyn. Adversarial examples from cryptographic pseudo-random generators. *arXiv preprint arXiv:1811.06418*, 2018.
- Sébastien Bubeck, Yin Tat Lee, Eric Price, and Ilya Razenshteyn. Adversarial examples from computational constraints. In *International Conference on Machine Learning*, pages 831–840. PMLR, 2019.
- Nicholas Carlini and David Wagner. Towards evaluating the robustness of neural networks. In *2017 IEEE Symposium on Security and Privacy (SP)*, pages 39–57. IEEE, 2017.
- Yair Carmon, Aditi Raghunathan, Ludwig Schmidt, John C Duchi, and Percy S Liang. Unlabeled data improves adversarial robustness. In *Advances in Neural Information Processing Systems*, pages 11192–11203, 2019.
- George Casella and Roger L Berger. *Statistical inference*. 1990.
- Olivier Chapelle, Jason Weston, Léon Bottou, and Vladimir Vapnik. Vicinal risk minimization. *Advances in neural information processing systems*, pages 416–422, 2001.
- Jeremy M Cohen, Elan Rosenfeld, and J Zico Kolter. Certified adversarial robustness via randomized smoothing. *arXiv preprint arXiv:1902.02918*, page arXiv:1902.02918, 2019.
- Francesco Croce and Matthias Hein. Reliable evaluation of adversarial robustness with an ensemble of diverse parameter-free attacks. In *International Conference on Machine Learning*, pages 2206–2216. PMLR, 2020.
- Francesco Croce, Maksym Andriushchenko, Vikash Sehwal, Nicolas Flammarion, Mung Chiang, Prateek Mittal, and Matthias Hein. Robustbench: a standardized adversarial robustness benchmark. *arXiv preprint arXiv:2010.09670*, 2020.
- Daniel Cullina, Arjun Nitin Bhagoji, and Prateek Mittal. Pac-learning in the presence of evasion adversaries. *arXiv preprint arXiv:1806.01471*, 2018.
- Chen Dan, Yuting Wei, and Pradeep Ravikumar. Sharp statistical guarantees for adversarially robust gaussian classification. In *ICML*, 2020.
- Edgar Dobriban, Hamed Hassani, David Hong, and Alexander Robey. Provable tradeoffs in adversarially robust classification. *arXiv preprint arXiv:2006.05161*, 2020.
- Elvis Dohmatob. Limitations of adversarial robustness: Strong no free lunch theorem. In *ICML*, 2019.
- Alhussein Fawzi, Omar Fawzi, and Pascal Frossard. Analysis of classifiers’ robustness to adversarial perturbations. *Machine Learning*, 107(3):481–508, 2018.

- Stuart Geman, Elie Bienenstock, and René Doursat. Neural networks and the bias/variance dilemma. *Neural computation*, 4(1):1–58, 1992.
- Justin Gilmer, Luke Metz, Fartash Faghri, Samuel S. Schoenholz, Maithra Raghu, Martin Wattenberg, and Ian Goodfellow. The relationship between high-dimensional geometry and adversarial examples, 2018. URL <http://arxiv.org/abs/1801.02774v3>.
- Ian J Goodfellow, Jonathon Shlens, and Christian Szegedy. Explaining and harnessing adversarial examples. *arXiv preprint arXiv:1412.6572*, 2014.
- Sven Gowal, Chongli Qin, Jonathan Uesato, Timothy Mann, and Pushmeet Kohli. Uncovering the limits of adversarial training against norm-bounded adversarial examples. *arXiv preprint arXiv:2010.03593*, 2020.
- Trevor Hastie, Robert Tibshirani, and Jerome Friedman. *The Elements of Statistical Learning; Data Mining, Inference and Prediction*. Springer, 2009.
- Trevor Hastie, Robert Tibshirani, and Martin Wainwright. *Statistical Learning with Sparsity: The Lasso and Generalizations*. CRC Press, 2015.
- Matthias Hein and Maksym Andriushchenko. Formal guarantees on the robustness of a classifier against adversarial manipulation. *arXiv preprint arXiv:1705.08475*, 2017.
- Dan Hendrycks and Thomas Dietterich. Benchmarking neural network robustness to common corruptions and perturbations. *arXiv preprint arXiv:1903.12261*, 2019.
- Dan Hendrycks, Norman Mu, Ekin D Cubuk, Barret Zoph, Justin Gilmer, and Balaji Lakshminarayanan. Augmix: A simple data processing method to improve robustness and uncertainty. *arXiv preprint arXiv:1912.02781*, 2019.
- Andrew Ilyas, Shibani Santurkar, Dimitris Tsipras, Logan Engstrom, Brandon Tran, and Aleksander Madry. Adversarial examples are not bugs, they are features. In *Advances in Neural Information Processing Systems*, pages 125–136, 2019.
- Adel Javanmard and Mahdi Soltanolkotabi. Precise statistical analysis of classification accuracies for adversarial training. *arXiv preprint arXiv:2010.11213*, 2020.
- Adel Javanmard, Mahdi Soltanolkotabi, and Hamed Hassani. Precise tradeoffs in adversarial training for linear regression. In *Conference on Learning Theory*, pages 2034–2078. PMLR, 2020.
- Daniel Kang, Yi Sun, Dan Hendrycks, Tom Brown, and Jacob Steinhardt. Testing robustness against unforeseen adversaries. *arXiv preprint arXiv:1908.08016*, 2019.
- Justin Khim and Po-Ling Loh. Adversarial risk bounds via function transformation. *arXiv preprint arXiv:1810.09519*, 2018.
- Diederik P Kingma and Jimmy Ba. Adam: A method for stochastic optimization. *arXiv preprint arXiv:1412.6980*, 2014.
- Alex Krizhevsky and Geoffrey Hinton. Learning multiple layers of features from tiny images. *0*, 2009.

- Alexey Kurakin, Ian Goodfellow, and Samy Bengio. Adversarial machine learning at scale. *arXiv preprint arXiv:1611.01236*, 2016.
- Mathias Lecuyer, Vaggelis Atlidakis, Roxana Geambasu, Daniel Hsu, and Suman Jana. Certified robustness to adversarial examples with differential privacy. In *2019 IEEE Symposium on Security and Privacy (SP)*, pages 656–672. IEEE, 2019.
- E.L. Lehmann. *Theory of point estimation*. Wiley series in probability and mathematical statistics: Probability and mathematical statistics. Wiley, 1983. URL <https://books.google.com/books?id=YdgwNZJ-YgUC>.
- Yan Li, Ethan X Fang, Huan Xu, and Tuo Zhao. Inductive bias of gradient descent based adversarial training on separable data. *arXiv preprint arXiv:1906.02931*, 2019.
- Licong Lin and Edgar Dobriban. What causes the test error? going beyond bias-variance via anova. *arXiv preprint arXiv:2010.05170*, 2020.
- Fanghui Liu, Zhenyu Liao, and Johan AK Suykens. Kernel regression in high dimension: Refined analysis beyond double descent. *arXiv preprint arXiv:2010.02681*, 2020.
- Yanpei Liu, Xinyun Chen, Chang Liu, and Dawn Song. Delving into transferable adversarial examples and black-box attacks. *arXiv preprint arXiv:1611.02770*, 2016.
- Aleksander Madry, Aleksandar Makelov, Ludwig Schmidt, Dimitris Tsipras, and Adrian Vladu. Towards deep learning models resistant to adversarial attacks. *arXiv preprint arXiv:1706.06083*, 2017.
- Saeed Mahloujifar, Xiao Zhang, Mohammad Mahmoody, and David Evans. Empirically measuring concentration: Fundamental limits on intrinsic robustness. In *Advances in Neural Information Processing Systems*, pages 5210–5221, 2019.
- A. Markov. *Wahrscheinlichkeitsrechnung*. Tebner, Leipzig, 1900.
- István Megyeri, István Hegedűs, and Márk Jelasity. Adversarial robustness of linear models: Regularization and dimensionality. In *ESANN 2019 - Proceedings, 27th European Symposium on Artificial Neural Networks, Computational Intelligence and Machine Learning*, pages 61–66, January 2019.
- Omar Montasser, Steve Hanneke, and Nathan Srebro. Vc classes are adversarially robustly learnable, but only improperly. *arXiv preprint arXiv:1902.04217*, 2019.
- Amir Najafi, Shin-ichi Maeda, Masanori Koyama, and Takeru Miyato. Robustness to adversarial perturbations in learning from incomplete data. *arXiv preprint arXiv:1905.13021*, 2019.
- Preetum Nakkiran. Adversarial robustness may be at odds with simplicity. *arXiv preprint arXiv:1901.00532*, 2019.
- Preetum Nakkiran, Gal Kaplun, Yamini Bansal, Tristan Yang, Boaz Barak, and Ilya Sutskever. Deep double descent: Where bigger models and more data hurt. In *International Conference on Learning Representations*, 2020. URL <https://openreview.net/forum?id=B1g5sA4twr>.
- Behnam Neyshabur, Ryota Tomioka, and Nathan Srebro. In search of the real inductive bias: On the role of implicit regularization in deep learning. *arXiv preprint arXiv:1412.6614*, 2014.

- Nicolas Papernot, Patrick McDaniel, Ian Goodfellow, Somesh Jha, Z Berkay Celik, and Ananthram Swami. Practical black-box attacks against machine learning. In *Proceedings of the 2017 ACM on Asia conference on computer and communications security*, pages 506–519, 2017.
- David Pfau. A generalized bias-variance decomposition for bregman divergences, 2013.
- Muni Sreenivas Pydi and Varun Jog. Adversarial risk via optimal transport and optimal couplings. In *ICML*, 2020.
- Aditi Raghunathan, Jacob Steinhardt, and Percy Liang. Certified defenses against adversarial examples. *arXiv preprint arXiv:1801.09344*, 2018.
- Aditi Raghunathan, Sang Michael Xie, Fanny Yang, John Duchi, and Percy Liang. Understanding and mitigating the tradeoff between robustness and accuracy. *arXiv preprint arXiv:2002.10716*, 2020.
- Benjamin Recht, Rebecca Roelofs, Ludwig Schmidt, and Vaishaal Shankar. Do cifar-10 classifiers generalize to cifar-10? *arXiv preprint arXiv:1806.00451*, 2018.
- Leslie Rice, Eric Wong, and J Zico Kolter. Overfitting in adversarially robust deep learning. *arXiv preprint arXiv:2002.11569*, 2020.
- Ludwig Schmidt, Shibani Santurkar, Dimitris Tsipras, Kunal Talwar, and Aleksander Madry. Adversarially robust generalization requires more data. In *Advances in Neural Information Processing Systems*, pages 5014–5026, 2018.
- Ali Shafahi, W. Ronny Huang, Christoph Studer, Soheil Feizi, and Tom Goldstein. Are adversarial examples inevitable? In *International Conference on Learning Representations*, 2019. URL <https://openreview.net/forum?id=r1lWUoA9FQ>.
- Harshay Shah, Kaustav Tamuly, Aditi Raghunathan, Prateek Jain, and Praneeth Netrapalli. The pitfalls of simplicity bias in neural networks. *arXiv preprint arXiv:2006.07710*, 2020.
- Aman Sinha, Hongseok Namkoong, Riccardo Volpi, and John Duchi. Certifying some distributional robustness with principled adversarial training. *arXiv preprint arXiv:1710.10571*, 2017.
- Christian Szegedy, Wojciech Zaremba, Ilya Sutskever, Joan Bruna, Dumitru Erhan, Ian Goodfellow, and Rob Fergus. Intriguing properties of neural networks. *arXiv preprint arXiv:1312.6199*, 2013.
- Hossein Taheri, Ramtin Pedarsani, and Christos Thrampoulidis. Asymptotic behavior of adversarial training in binary classification. *arXiv preprint arXiv:2010.13275*, 2020.
- Florian Tramèr, Alexey Kurakin, Nicolas Papernot, Ian Goodfellow, Dan Boneh, and Patrick McDaniel. Ensemble adversarial training: Attacks and defenses. *arXiv preprint arXiv:1705.07204*, 2017.
- Dimitris Tsipras, Shibani Santurkar, Logan Engstrom, Alexander Turner, and Aleksander Madry. Robustness may be at odds with accuracy. *arXiv preprint arXiv:1805.12152*, 2018.
- Jonathan Uesato, Jean-Baptiste Alayrac, Po-Sen Huang, Robert Stanforth, Alhussein Fawzi, and Pushmeet Kohli. Are labels required for improving adversarial robustness? *arXiv preprint arXiv:1905.13725*, 2019.

- Yizhen Wang, Somesh Jha, and Kamalika Chaudhuri. Analyzing the robustness of nearest neighbors to adversarial examples. In *International Conference on Machine Learning*, pages 5133–5142, 2018.
- Eric Wong and J Zico Kolter. Provable defenses against adversarial examples via the convex outer adversarial polytope. *arXiv preprint arXiv:1711.00851*, 2017.
- Yue Xing, Ruizhi Zhang, and Guang Cheng. Adversarially robust estimate and risk analysis in linear regression, 2020.
- Huan Xu, Constantine Caramanis, and Shie Mannor. Robust regression and lasso. In *Advances in Neural Information Processing Systems*, pages 1801–1808, 2009a.
- Huan Xu, Constantine Caramanis, and Shie Mannor. Robustness and regularization of support vector machines. *Journal of machine learning research*, 10(Jul):1485–1510, 2009b.
- Yao-Yuan Yang, Cyrus Rashtchian, Yizhen Wang, and Kamalika Chaudhuri. Robustness for non-parametric classification: A generic attack and defense. In *International Conference on Artificial Intelligence and Statistics*, pages 941–951, 2020a.
- Yao-Yuan Yang, Cyrus Rashtchian, Hongyang Zhang, Ruslan Salakhutdinov, and Kamalika Chaudhuri. A closer look at accuracy vs. robustness. *arXiv preprint arXiv:2003.02460*, 2020b.
- Zitong Yang, Yaodong Yu, Chong You, Jacob Steinhardt, and Yi Ma. Rethinking Bias-Variance Trade-off for Generalization of Neural Networks. *arXiv e-prints*, art. arXiv:2002.11328, February 2020.
- Dong Yin, Ramchandran Kannan, and Peter Bartlett. Rademacher complexity for adversarially robust generalization. In *International Conference on Machine Learning*, pages 7085–7094. PMLR, 2019.
- Sergey Zagoruyko and Nikos Komodakis. Wide residual networks. *arXiv preprint arXiv:1605.07146*, page arXiv:1605.07146, 2016.
- Runtian Zhai, Tianle Cai, Di He, Chen Dan, Kun He, John Hopcroft, and Liwei Wang. Adversarially robust generalization just requires more unlabeled data. *arXiv preprint arXiv:1906.00555*, 2019.
- Hongyang Zhang, Yaodong Yu, Jiantao Jiao, Eric P Xing, Laurent El Ghaoui, and Michael I Jordan. Theoretically principled trade-off between robustness and accuracy. *arXiv preprint arXiv:1901.08573*, 2019.

A Algorithm for Estimating Bias-variance

In this section, we present the algorithm for estimating the (*adversarial*) variance for squared loss. Also, we introduce the *adversarial* bias-variance decomposition for cross-entropy loss.

A.1 Algorithm for Estimating the Variance

The algorithm for estimating the variance is described in Algorithm 1. The adversarial variance and bias can be estimated as follows:

$$\begin{aligned}\widehat{\text{AVar}} &= \mathbb{E}_{\mathbf{x}, \mathbf{y}} \left[\widehat{\text{AVar}}(\mathbf{x}, \mathbf{y}) \right], \\ \widehat{\text{ABias}} &= \frac{1}{K} \sum_{k=1}^K \mathbb{E}_{\mathcal{T}^{(k)}} \mathbb{E}_{\mathbf{x}, \mathbf{y}} \left[\max_{\boldsymbol{\delta} \in \Delta} \left\| f_{\hat{\boldsymbol{\theta}}(\mathcal{T}^{(k)})}(\mathbf{x} + \boldsymbol{\delta}) - \mathbf{y} \right\|^2 \right] - \widehat{\text{AVar}},\end{aligned}\tag{8}$$

where $\widehat{\text{AVar}}(\mathbf{x}, \mathbf{y})$ is calculated by Algorithm 1. We can also apply Eq. (8) for evaluating the standard bias and variance by setting $\varepsilon = 0$ for the perturbation set $\Delta = \{\boldsymbol{\delta} : \|\boldsymbol{\delta}\|_p \leq \varepsilon\}$.

Algorithm 1 Estimating Adversarial Variance for Squared Loss

Input: Test point (\mathbf{x}, \mathbf{y}) , Training set \mathcal{T} , Number of repetitions K .

for $k = 1$ **to** K **do**

 Split \mathcal{T} into $\mathcal{T}_1^{(k)}, \dots, \mathcal{T}_N^{(k)}$.

for $j = 1$ **to** N **do**

 Perform adversarial training on training dataset $\mathcal{T}_j^{(k)}$;

 Find $\hat{\boldsymbol{\theta}}(\mathcal{T}_j^{(k)})$ that approximately solves $\left\{ \min_{\boldsymbol{\theta}} \frac{1}{|\mathcal{T}_j^{(k)}|} \sum_{i \in \mathcal{T}_j^{(k)}} \max_{\boldsymbol{\delta}_i \in \Delta} \ell(f_{\boldsymbol{\theta}}(\mathbf{x}_i + \boldsymbol{\delta}_i), \mathbf{y}_i) \right\}$;

 Find adversarial perturbation $\boldsymbol{\delta}(\mathbf{x}, \mathbf{y}, \mathcal{T}_j^{(k)})$ that approximately solves

$$\left\{ \max_{\boldsymbol{\delta} \in \Delta} \ell \left(f_{\hat{\boldsymbol{\theta}}(\mathcal{T}_j^{(k)})}(\mathbf{x} + \boldsymbol{\delta}), \mathbf{y} \right) \right\};$$

end for

end for

for $k = 1$ **to** K **do**

 Compute

$$\widehat{\text{AVar}}(\mathbf{x}, \mathbf{y}, \mathcal{T}^{(k)}) = \frac{1}{N-1} \sum_{j=1}^N \left\| f_{\hat{\boldsymbol{\theta}}(\mathcal{T}_j^{(k)})}(\mathbf{x} + \boldsymbol{\delta}(\mathbf{x}, \mathbf{y}, \mathcal{T}_j^{(k)})) - \frac{1}{N} \sum_{j=1}^N f_{\hat{\boldsymbol{\theta}}(\mathcal{T}_j^{(k)})}(\mathbf{x} + \boldsymbol{\delta}(\mathbf{x}, \mathbf{y}, \mathcal{T}_j^{(k)})) \right\|_2^2;$$

end for

 Compute $\widehat{\text{AVar}}(\mathbf{x}, \mathbf{y}) = \frac{1}{K} \sum_{k=1}^K \widehat{\text{AVar}}(\mathbf{x}, \mathbf{y}, \mathcal{T}^{(k)})$.

A.2 Bias-variance Decomposition for Cross-entropy Loss

Inspired by Pfau [2013], Yang et al. [2020] provides a bias-variance decomposition for cross-entropy loss. We also extend their decomposition to the adversarial setting. We use boldface \mathbf{f} instead of f to

emphasize that $\mathbf{f}_\theta \in \mathbb{R}^c$ is now a vector that represents a probability distribution over the class labels, i.e., $\sum_{i=1}^c \mathbf{f}_\theta(x)_i = 1$. We are given a trained model $\hat{\theta}(\mathcal{T})$, a test point $(\mathbf{x}, \mathbf{y}) \in \mathbb{R}^d \times \mathbb{R}^c$, where \mathbf{y} is the one-hot encoding of the class membership of input \mathbf{x} . We first compute the worst-case perturbation as

$$\delta(\mathbf{x}, \mathbf{y}, \mathcal{T}) \in \arg \max_{\delta \in \Delta} \{H(\mathbf{f}_{\hat{\theta}}(\mathbf{x} + \delta), \mathbf{y})\},$$

where $H(\mathbf{a}, \mathbf{b}) = -\sum_{i=1}^c \mathbf{a}_i \log(\mathbf{b}_i)$ is the standard cross-entropy loss. At the adversarially perturbed test point $\mathbf{x}' = \mathbf{x}'(\mathbf{x}, \mathbf{y}, \mathcal{T}) = \mathbf{x} + \delta(\mathbf{x}, \mathbf{y}, \mathcal{T})$, we define the average prediction $\bar{\mathbf{f}}$ at \mathbf{x}' as

$$\bar{\mathbf{f}}_i \propto \exp[\mathbb{E}_{\mathcal{T}} \log \mathbf{f}_{\hat{\theta}}(\mathbf{x}')_i], \quad i \in [c], \quad \text{and} \quad \sum_{i=1}^c \bar{\mathbf{f}}_i = 1.$$

Now we are ready to state the formula for the adversarial ‘‘bias-variance’’ decomposition of the cross-entropy loss:

$$\underbrace{\mathbb{E}_{\mathcal{T}} \mathbb{E}_{\mathbf{x}, \mathbf{y}} \left[\max_{\delta \in \Delta} H(\mathbf{f}_{\hat{\theta}(\mathcal{T})}(\mathbf{x} + \delta), \mathbf{y}) \right]}_{\text{Adversarial Risk (CE)}} = \mathbb{E}_{\mathbf{x}, \mathbf{y}} \mathbb{E}_{\mathcal{T}} H(\mathbf{f}_{\hat{\theta}(\mathcal{T})}(\mathbf{x} + \delta(\mathbf{x}, \mathbf{y}, \mathcal{T})), \mathbf{y}) + \underbrace{\mathbb{E}_{\mathbf{x}, \mathbf{y}} D_{\text{KL}}(\mathbf{y} \parallel \bar{\mathbf{f}})}_{\text{Adversarial Bias (CE)}}. \quad (9)$$

The standard bias and variance can be computed analogously.

B Additional Experiments on Adversarial Logistic Regression

In this subsection, we present additional experiments on adversarial logistic regression. The precise setup of the experiments is defined in Section 4. We consider $(n = 100, d = 120)$ and $(n = 100, d = 50)$ for the adversarial logistic regression. As shown in Figure 8, the variance is unimodal and the variance peak is close to the interpolation threshold. In Figure 7(b) and 8, the training error denotes the standard training error.

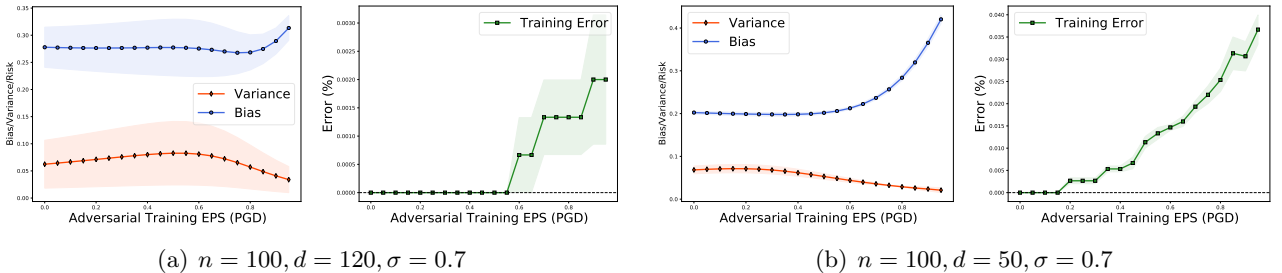


Figure 8: More results on the relation between bias/variance/interpolation threshold for adversarial logistic regression. The only distinction is that (a) $d = 120$, (b) $d = 50$. We can see that the variance peak corresponds closely to the interpolation threshold.

C Additional Experiments for Deep Neural Networks

In this section, we provide additional experimental results details related to Section 3. Specifically, we provide the detailed experimental setup for Gaussian noise training in Section C.1. In Section C.2,

we present additional experimental results for the ℓ_2 and ℓ_∞ adversarial training on CIFAR10 and CIFAR100 datasets. We also study the effect of the width factor in adversarial training. In Section C.3, we study the bias and variance of deep models on out-of-distribution (OOD) datasets. In Section C.4, we evaluate the (*cross-entropy loss*) bias and variance for ℓ_∞ and ℓ_2 adversarially trained models on the CIFAR10 dataset.

C.1 Experimental setup for training with Gaussian Noise

Experimental setup. For randomized smoothing training, following previous works [Lecuyer et al., 2019, Cohen et al., 2019], we train the models with additive Gaussian data augmentation with variance σ^2 on the CIFAR10 dataset. The variance σ^2 is chosen as $\sigma \in \{k \cdot 0.125 : k = 0, \dots, 8\}$. After adding noise to the input, we clip the pixels to $[0.0, 1.0]$. For training on Gaussian-perturbed data, we perturb the training images from CIFAR10 with random additive Gaussian noise with variance σ^2 , where $\sigma \in \{k \cdot 0.125 : k = 0, \dots, 8\}$, then clip pixels to $[0.0, 1.0]$ and save the images using the standard JPEG compression. The same architecture (WRN-28-10) and optimization procedure are applied for randomized smoothing training and training on Gaussian-perturbed data as for ℓ_∞ adversarial training, described earlier. The **robust error** (in Figure 3(a)) of randomized smoothing trained models is evaluated by adding random Gaussian noise (with the same variance σ^2 as in training) to the training dataset.

C.2 Additional Experiments on Measure Bias-variance of Adversarial Training models on CIFAR10/100

For ℓ_2 adversarial training, we apply a 10-step (ℓ_2) PGD attack with perturbation step size $\eta = 0.25 \cdot (\varepsilon/255)$.

ℓ_2 adversarial training on CIFAR10. We first study the bias-variance decomposition of ℓ_2 adversarially trained models on the CIFAR10 dataset. We summarize the results in Figure 9. The bias and variance of ℓ_2 adversarially trained models are similar to the ones in ℓ_∞ adversarial training (in Figure 1(b)). We find that the variance is unimodal and the bias is monotonically increasing with the perturbation size. Also, the variance peak is near the robust interpolation threshold.

Results on CIFAR100. In Figure 10 and Figure 11, we study the bias-variance behavior on the CIFAR100 dataset. Following Rice et al. [2020], we use pre-activation ResNet18 (PreResNet-18) architecture for the CIFAR100 dataset and apply the same training parameters as used for CIFAR10. We find that, on the CIFAR100 dataset, the variance is indeed unimodal, the bias dominates the risk and monotonically increasing, and the peak of the variance is close to the robust interpolation threshold. The results for bias and variance on the CIFAR100 dataset are similar to the ones on the CIFAR10 dataset.

Effect of width factor. We study the effect of the width factor of the WideResNet-28 in ($\ell = 8.0/255.0$) adversarial training on the CIFAR10 dataset. We apply the same training parameters as mentioned in Section 3.1 and only change the wide factor of WideResNet-28 from 1 to 20. As shown in Figure 12, the variance changes monotonicity at the interpolation threshold (**width=4**). We observe that the bias is monotonically decreasing with the width factor. The variance is increasing before the robust interpolation threshold. After the threshold, the variance value does not change too much.

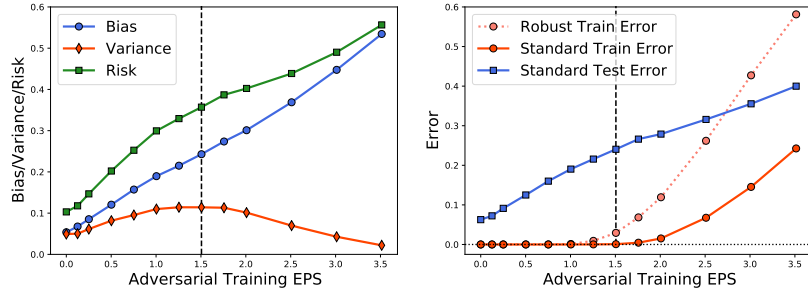


Figure 9: Measuring performance for $(\ell_2 = \varepsilon)$ -adversarial training (with increasing perturbation size) on *CIFAR10* dataset. **(left)** Evaluating bias, variance, and risk for the ℓ_2 -adversarially trained models (WideResNet-28-10) on the *CIFAR10* dataset. **(right)** Evaluating robust training error, standard training/test error for the ℓ_2 -adversarially trained models (WideResNet-28-10) on the *CIFAR10* dataset.

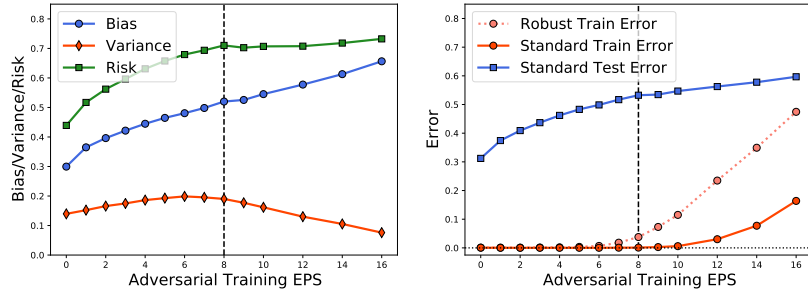


Figure 10: Measuring performance for $(\ell_\infty = \varepsilon/255.0)$ -adversarial training (with increasing perturbation size) on *CIFAR100* dataset. **(left)** Evaluating bias, variance, and risk for the ℓ_∞ -adversarially trained models (PreResNet-18) on the *CIFAR100* dataset. **(right)** Evaluating robust training error, standard training/test error for the ℓ_∞ -adversarially trained models (PreResNet-18) on the *CIFAR100* dataset.

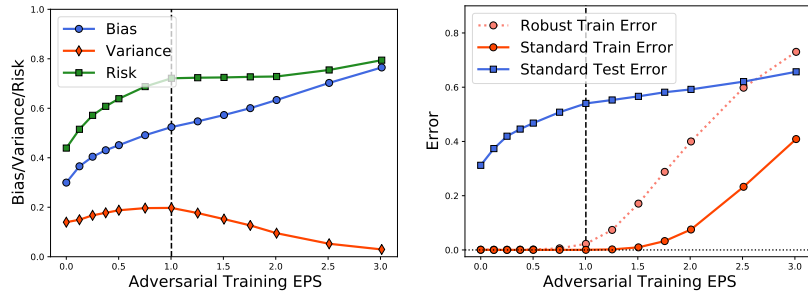


Figure 11: Measuring performance for $(\ell_2 = \varepsilon)$ -adversarial training (with increasing perturbation size) on *CIFAR100* dataset. **(left)** Evaluating bias, variance, and risk for the ℓ_2 -adversarially trained models (PreResNet-18) on the *CIFAR100* dataset. **(right)** Evaluating robust training error, standard training/test error for the ℓ_2 -adversarially trained models (PreResNet-18) on the *CIFAR100* dataset.

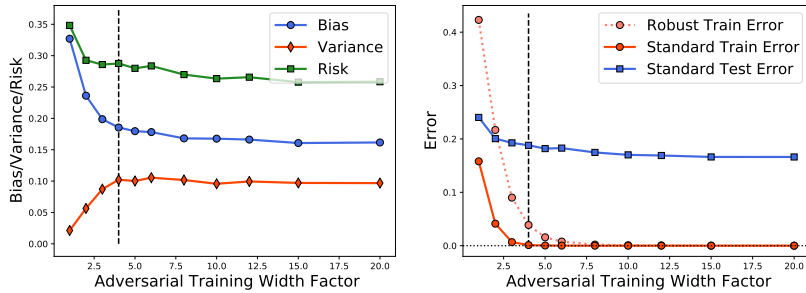


Figure 12: Measuring performance for ($\ell_\infty = 8.0/255.0$)-adversarial training (with increasing width factor for WideResNet-28-[width]) on *CIFAR10* dataset. **(left)** Evaluating bias, variance, and risk for the ($\ell_\infty = 8.0/255.0$)-adversarially trained models (WideResNet-28-[width]) on the *CIFAR10* dataset. **(right)** Evaluating robust training error, standard training/test error for the ℓ_∞ -adversarially trained models (WideResNet-28-[width]) on the *CIFAR10* dataset.

C.3 Measuring Bias-variance of Adversarial Training Models on OOD datasets.

We study the bias-variance decomposition for ℓ_∞ -adversarially trained models and AugMix [Hendrycks et al., 2019]-trained models (on the CIFAR10 dataset) evaluated on datasets under distributional shift. This includes natural distributional shift, in the CIFAR10-v6 dataset [Recht et al., 2018], and a common corruption benchmark, the CIFAR10-C dataset [Hendrycks and Dietterich, 2019].

CIFAR10-C results. CIFAR10-C contains 15 different common corruptions with 5 levels of severity. We evaluate the bias and variance on test samples with different severity levels. As shown in Figure 13, we observe that the bias curve becomes U-shaped on CIFAR10-C and the variance curve changes to a “double-descent-shaped” curve (with two dips) when evaluated on out-of-distribution data. The differences in the variance across different severity levels become small when the perturbation radius ε is large. Another observation is that when the adversarial perturbation radius ε is small, both the bias and variance of the adversarially trained models are *smaller* than standard-trained models on the CIFAR10-C dataset. This suggests that the adversarial training with small perturbation radii may help with common corruption robustness because adversarial training can reduce both bias and variance on OOD datasets.

CIFAR10-v6 results. CIFAR10-v6 contains new collected test images for the CIFAR10 dataset. The results of ℓ_∞ -adversarial training on CIFAR10-v6 are summarized in Figure 14. We find that the bias and variance on CIFAR10-v6 are similar to the standard test dataset case (in Figure 1(b)), whereas the variance decreases after $\varepsilon = 10$.

AugMix training. In addition, we study the bias-variance decomposition for AugMix training on the CIFAR10 dataset. We change the severity (augmentation severity parameter in AugMix) from 0 to 10, where 0 corresponds to the standard training and 10 is the maximum severity defined in AugMix. We summarize the bias-variance decomposition results in Figure 15. For AugMix training, we find that bias, variance, and risk are monotonically decreasing with increased augmentation severity. The bias-variance behavior of AugMix training is different from ℓ_∞ -adversarial training (in Figure 13).

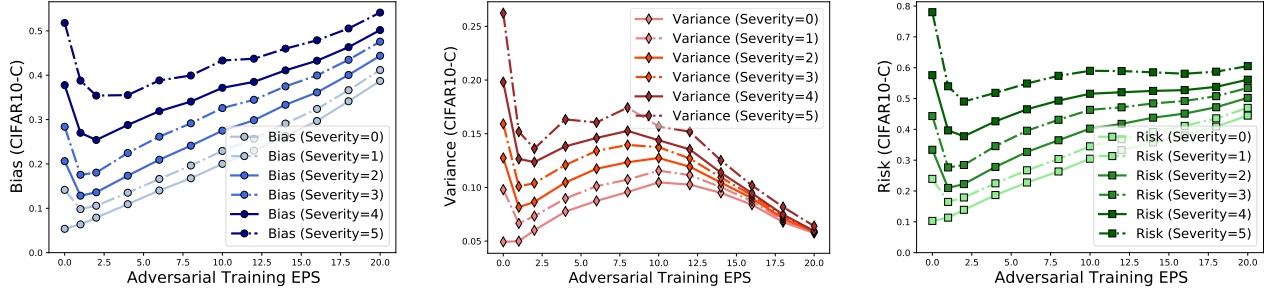


Figure 13: Bias, variance, and risk for ℓ_∞ -adversarial training models evaluated on the CIFAR10-C dataset with different severity. Each curve corresponds to one level of severity, and severity=0 corresponds to the standard test CIFAR10 testset. **(Left)** Bias. **(Middle)** Variance. **(Right)** Risk.

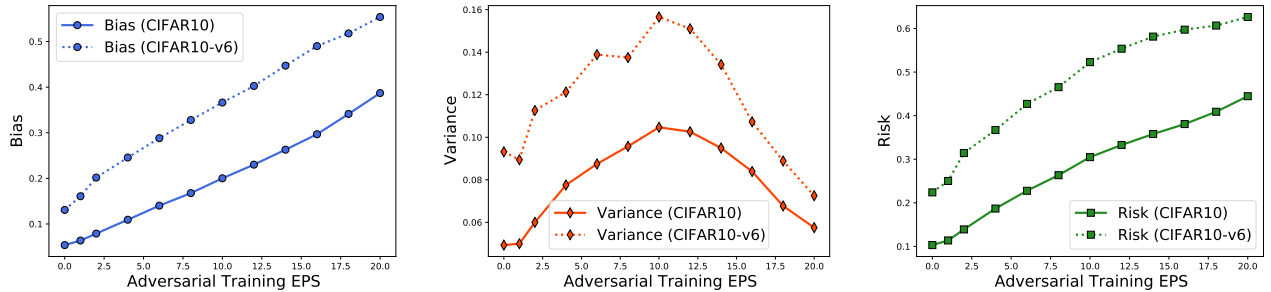


Figure 14: Compare bias, variance, and risk for ℓ_∞ -adversarial training models evaluated on the CIFAR10-v6 and standard CIFAR10 testset. **(Left)** Bias. **(Middle)** Variance. **(Right)** Risk.

C.4 Measuring Bias-variance Decomposition for Cross-Entropy Loss.

We study the bias-variance decomposition for cross-entropy (CE) loss defined above. We follow Algorithm 1 in Yang et al. [2020] to evaluate the bias and variance for the cross-entropy loss. Specifically, we evaluate the (*cross-entropy loss*) bias-variance decomposition for ℓ_∞ -adversarially trained models (as shown in Figure 16) and ℓ_2 -adversarially trained models (shown in Figure 17) on the CIFAR10 dataset. From Figure 16 and Figure 17, we observe the unimodal variance curve and monotonically increasing bias curve for the (*cross-entropy loss*) bias-variance decomposition. The peak of the (*cross-entropy loss*) variance is also near the robust interpolation threshold.

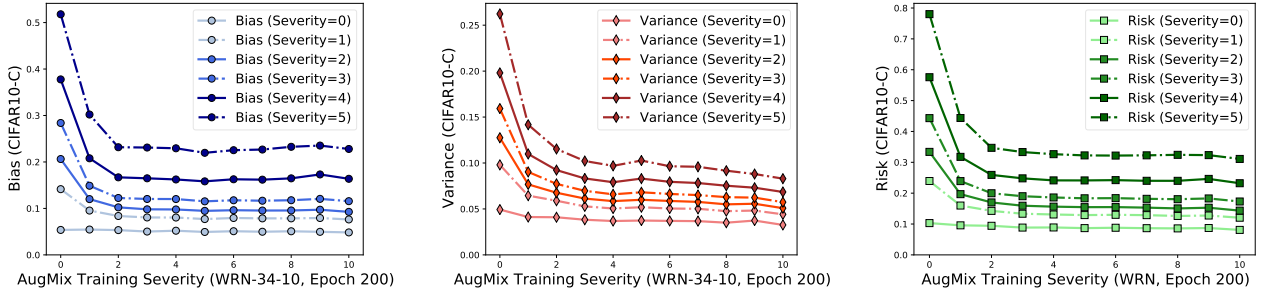


Figure 15: Bias, variance, and risk for AugMix training models (without applying JSD loss) evaluated on the CIFAR10-C dataset with different severity. Each curve corresponds to one level of severity, and severity=0 corresponds to the standard test CIFAR10 testset. **(Left)** Bias. **(Middle)** Variance. **(Right)** Risk.

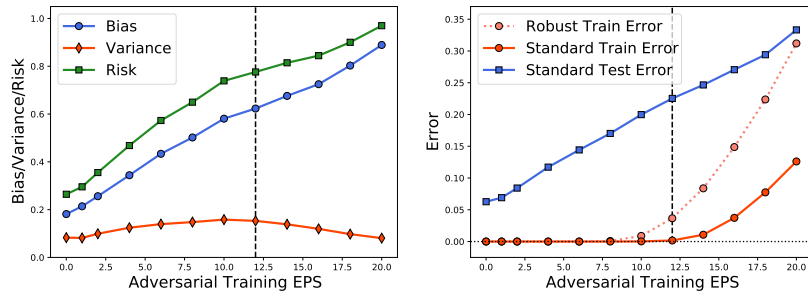


Figure 16: Measuring performance for ($\ell_\infty = \varepsilon/255.0$)-adversarial training (with increasing perturbation size) on *CIFAR10* dataset. **(left)** Evaluating (*cross-entropy loss*) bias, variance, and risk for the ℓ_∞ -adversarially trained models (WideResNet-28-10) on the *CIFAR10* dataset. **(right)** Evaluating robust training error, standard training/test error for the ℓ_∞ -adversarially trained models (WideResNet-28-10) on the *CIFAR10* dataset.

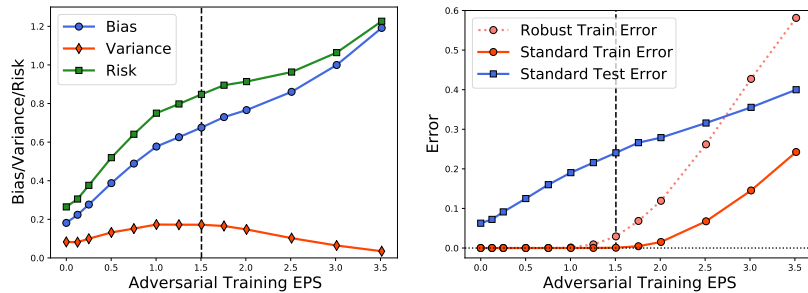


Figure 17: Measuring performance for ($\ell_2 = \varepsilon$)-adversarial training (with increasing perturbation size) on *CIFAR10* dataset. **(left)** Evaluating (*cross-entropy loss*) bias, variance, and risk for the ℓ_2 -adversarially trained models (WideResNet-28-10) on the *CIFAR10* dataset. **(right)** Evaluating robust training error, standard training/test error for the ℓ_2 -adversarially trained models (WideResNet-28-10) on the *CIFAR10* dataset.

D Bias and Variance for Logistic Regression

In this section, we present the bias-variance decomposition for logistic loss. We also prove that the logistic variance satisfies the usual properties of the variance.

D.1 Definitions

Let $\mathcal{C} = \{\pm 1\}$ be the set of classes. Then, the label $y \in \mathcal{C}$ defines a probability distribution π on \mathcal{C} as

$$\pi_y(c) = \frac{1}{2}(1 + cy).$$

Similarly, given test data \mathbf{x} and learned parameter $\hat{\boldsymbol{\theta}}_n$, the classification rule defines a distribution $\hat{\pi}$ on \mathcal{C} as

$$\hat{\pi}_{\mathbf{x}, \hat{\boldsymbol{\theta}}_n}(c) = \left(1 + e^{-c\langle \mathbf{x}, \hat{\boldsymbol{\theta}}_n \rangle}\right)^{-1}.$$

Since $\hat{\boldsymbol{\theta}}_n$ is random, $\hat{\pi}$ is also a random distribution. The logistic loss can equivalently be written in terms of the cross-entropy between π and $\hat{\pi}$: $H(\pi_y, \hat{\pi}_{\mathbf{x}, \hat{\boldsymbol{\theta}}_n})$

$$\begin{aligned} \mathbf{R}(\hat{\boldsymbol{\theta}}_n) &= \mathbb{E}_{\mathbf{x}, y} \ell(y \langle \hat{\boldsymbol{\theta}}_n, \mathbf{x} \rangle) \\ &= \mathbb{E}_{\mathbf{x}, y} \left[\log \left(1 + e^{-y \langle \hat{\boldsymbol{\theta}}_n, \mathbf{x} \rangle}\right) \right], \\ &= \mathbb{E}_{\mathbf{x}, y} \left[- \sum_c \pi_y(c) \log \hat{\pi}_{\mathbf{x}, \hat{\boldsymbol{\theta}}_n}(c) \right] \\ &= \mathbb{E}_{\mathbf{x}, y} \left[H(\pi_y, \hat{\pi}_{\mathbf{x}, \hat{\boldsymbol{\theta}}_n}) \right], \\ &= \mathbb{E}_{\mathbf{x}, y} \left[H(\pi_y) + D(\pi_y \| \hat{\pi}_{\mathbf{x}, \hat{\boldsymbol{\theta}}_n}) \right], \\ &= \mathbb{E}_{\mathbf{x}, y} \left[D(\pi_y \| \hat{\pi}_{\mathbf{x}, \hat{\boldsymbol{\theta}}_n}) \right], \end{aligned}$$

where $D(\cdot \| \cdot)$ denotes the KL divergence. In [Yang et al. \[2020\]](#), the following bias-variance decomposition is given for the cross-entropy loss:

$$\begin{aligned} &\mathbb{E}_{\mathbf{x}, y} \mathbb{E}_{\hat{\boldsymbol{\theta}}_n} \left[D(\pi_y \| \hat{\pi}_{\mathbf{x}, \hat{\boldsymbol{\theta}}_n}) \right] \\ &= \mathbb{E}_{\mathbf{x}, y} D(\pi_y \| \boldsymbol{\pi}_{\mathbf{x}}) + \mathbb{E}_{\mathbf{x}, y} \mathbb{E}_{\hat{\boldsymbol{\theta}}_n} D(\boldsymbol{\pi}_{\mathbf{x}} \| \hat{\pi}_{\mathbf{x}, \hat{\boldsymbol{\theta}}_n}), \end{aligned}$$

where $\boldsymbol{\pi}_{\mathbf{x}}$ is the average of log probability:

$$\boldsymbol{\pi}_{\mathbf{x}}(c) = \frac{e^{\mathbb{E}_{\hat{\boldsymbol{\theta}}_n} \log \hat{\pi}_{\mathbf{x}, \hat{\boldsymbol{\theta}}_n}(c)}}}{Z_{\mathbf{x}}} = \frac{\exp \left[-\mathbb{E}_{\hat{\boldsymbol{\theta}}_n} \ell(c \langle \hat{\boldsymbol{\theta}}_n, \mathbf{x} \rangle) \right]}{Z_{\mathbf{x}}},$$

where

$$Z_{\mathbf{x}} = \exp \left[-\mathbb{E}_{\hat{\boldsymbol{\theta}}_n} \ell(\langle \hat{\boldsymbol{\theta}}_n, \mathbf{x} \rangle) \right] + \exp \left[-\mathbb{E}_{\hat{\boldsymbol{\theta}}_n} \ell(-\langle \hat{\boldsymbol{\theta}}_n, \mathbf{x} \rangle) \right]$$

is the normalization factor. Then, the bias term is

$$\begin{aligned} \text{Bias} &= \mathbb{E}_{\mathbf{x}, y} \left[\sum_c \pi_y(c) \log \frac{\pi_y(c)}{\boldsymbol{\pi}_{\mathbf{x}}(c)} \right], \\ &= \mathbb{E}_{\mathbf{x}, y} \left[\log Z_{\mathbf{x}} + \mathbb{E}_{\hat{\boldsymbol{\theta}}_n} \ell(y \langle \hat{\boldsymbol{\theta}}_n, \mathbf{x} \rangle) \right]. \end{aligned}$$

Notice that

$$\text{Bias} = \mathbb{E}_{\mathbf{x}, y} \log Z_{\mathbf{x}} + \mathbb{E}_{\hat{\boldsymbol{\theta}}_n} R(\hat{\boldsymbol{\theta}}_n). \quad (10)$$

Thus, the above calculation also identifies

$$\text{Variance} = -\mathbb{E}_{\mathbf{x}} \log Z_{\mathbf{x}}. \quad (11)$$

D.2 Properties of Logistic Variance

The proposition below shows that the variance for logistic regression has the usual non-negativity property of the variance; as expected.

Proposition 3 (Non-Negativity of Logistic Variance). *The variance for logistic regression defined in (11) is non-negative, and equals 0 when the learned parameters $\hat{\boldsymbol{\theta}}_n$ is non-random.*

Proof. First, we evaluate the formula for the limiting case when the sample size diverges to infinity. This is used later to prove non-negativity. Suppose that as $n \rightarrow \infty$, the estimate $\hat{\boldsymbol{\theta}}_n$ concentrates around some value $\boldsymbol{\theta}_*$ (which of course can depend on the objective function, and in particular on ε for adversarial robustness). Then, $Z_{\mathbf{x}}$ is approximated by

$$\begin{aligned} Z_{\mathbf{x}}^* &= \exp[-\ell(\langle \boldsymbol{\theta}_*, \mathbf{x} \rangle)] + \exp[-\ell(-\langle \boldsymbol{\theta}_*, \mathbf{x} \rangle)] \\ &= \exp\left[-\log\left(1 + e^{-\langle \boldsymbol{\theta}_*, \mathbf{x} \rangle}\right)\right] + \exp\left[-\log\left(1 + e^{\langle \boldsymbol{\theta}_*, \mathbf{x} \rangle}\right)\right] \\ &= \left(1 + e^{-\langle \boldsymbol{\theta}_*, \mathbf{x} \rangle}\right)^{-1} + \left(1 + e^{\langle \boldsymbol{\theta}_*, \mathbf{x} \rangle}\right)^{-1} = 1. \end{aligned}$$

Therefore, we have $\text{Variance} \rightarrow 0$ asymptotically. Since the log-sum-exp function $L(z_1, \dots, z_m) = \log(\sum \exp z_i)$ is convex, it follows from Jensen's inequality that

$$\begin{aligned} \log Z_{\mathbf{x}} &= \log\left(\exp\left[-\mathbb{E}_{\hat{\boldsymbol{\theta}}_n} \ell(\langle \hat{\boldsymbol{\theta}}_n, \mathbf{x} \rangle)\right] + \exp\left[-\mathbb{E}_{\hat{\boldsymbol{\theta}}_n} \ell(-\langle \hat{\boldsymbol{\theta}}_n, \mathbf{x} \rangle)\right]\right) \\ &= L\left(-\mathbb{E}_{\hat{\boldsymbol{\theta}}_n} \ell(\langle \hat{\boldsymbol{\theta}}_n, \mathbf{x} \rangle), -\mathbb{E}_{\hat{\boldsymbol{\theta}}_n} \ell(-\langle \hat{\boldsymbol{\theta}}_n, \mathbf{x} \rangle)\right) \\ &\geq \mathbb{E}_{\hat{\boldsymbol{\theta}}_n} L\left(-\ell(\langle \hat{\boldsymbol{\theta}}_n, \mathbf{x} \rangle), -\ell(-\langle \hat{\boldsymbol{\theta}}_n, \mathbf{x} \rangle)\right) \\ &= \mathbb{E}_{\hat{\boldsymbol{\theta}}_n} 0 = 0. \end{aligned}$$

Hence, $Z_{\mathbf{x}} \geq 1$ and the above notion of variance is non-negative, $\text{Variance} \geq 0$. □